American Mineralogist, Volume 106, pages 1438–1452, 2021

Plagioclase population dynamics and zoning in response to changes in temperature and pressure

Benjamin J. Andrews[1,*]

[1]Global Volcanism Program, Smithsonian Institution, Washington, D.C. 20560, U.S.A.

Abstract

Zoned plagioclase crystals are often interpreted as proxies for magmatic history because the mineral is present in most silicic magmas and has compositional sensitivity to magmatic conditions (pressure, temperature, and composition) with slow internal diffusion that preserves compositional zones. Changes in growth rates and crystal dissolution present challenges to quantitatively relating time to particular zoning patterns. The numerical model SNGPlag uses Rhyolite MELTS to determine the equilibrium phase assemblage and compositions for a user-defined magma composition experimentally determined instantaneous nucleation and growth rates, and reasonable dissolution rates to examine plagioclase crystallization and population dynamics through time. The model tracks the numbers, sizes, morphologies, and compositional zoning of plagioclase crystals through time in response to changes in pressure, temperature, and volume or mass inputs. Model results show that significant fractions of time are functionally missing from the crystal record because of effectively zero growth rates or erased from the record through dissolution; in some instances, those processes can together remove >>50% of time from the crystal record. The results show that temperature- (or pressure-) cycling alone will not produce substantial compositional zoning but that the addition of new magma is required to grow complexly zoned phenocrysts. Comparison of the input pressure-temperature-time series with compositional transects shows that the crystal record is biased toward more recent intervals and periods of decreasing temperature (i.e., neither the peak temperatures nor intervals of prolonged, cool storage are favored). Crystallization (or dissolution during heating) acts to return magmas to near-equilibrium crystal fractions within hundreds of days.

Keywords: Plagioclase, zoning, nucleation, growth, dissolution, numerical model, crystal population

Introduction

Volcanic rocks provide the only record of magmatic processes for all ancient or prehistoric eruptions and at most presently active volcanoes, the exceptions being the relative handful of monitored volcanoes and studies with modern geophysical instruments. Fractional crystallization, magma recharge and mixing, and crustal assimilation all affect the composition and phase assemblage of a magma. The bulk chemical and isotopic compositions of rock and glass can provide an integrative record of magmatic events preceding eruption. Certain mineral phases tend to develop and maintain compositional zoning that records changes in magmatic conditions; each crystal is thus a potentially high-resolution time-series record of magmatic processes.

Plagioclase is often used to interpret pre-eruptive magmatic processes as it is a generally abundant phenocryst phase common to many volcanic systems. Numerous workers have used compositional and/or isotopic zoning together with phenocryst textures to interpret changes in pressure and temperature, or magma recharge and mixing (e.g., Gerlach and Grove 1982; Anderson 1984; Tsuchiyama 1985; Singer et al. 1995; Davidson and Tepley 1997; Tepley et al. 1999, 2000; Davidson et al. 2001; Costa et al. 2003, 2008; Browne et al. 2006; Andrews et al. 2008; Salisbury et al. 2008; Streck et al. 2008; Waters et al. 2015). U-series geochronometry has been applied to zoned crystals, typically zircons, from some magmas to quantitatively constrain the timescales of at least a portion of the magmatic histories recorded by individual crystals (Cooper and Reid 2003; Cooper and Kent 2014; Budd et al. 2017). All of those studies rely upon the core-to-rim growth of the crystals to relate compositional changes in the crystals to temporal evolution of the magmatic systems. Unfortunately, many crystals show evidence of dissolution; thus the records they contain are not complete and the degree to which they are incomplete is largely unknown. This observation, coupled with the variability of crystal growth rates as a function of pressure, temperature, and supersaturation (Hammer and Rutherford 2002; Mollard, et al. 2012; Befus and Andrews 2018), results in substantial challenges to quantitative relation of time to particular zoning patterns (Fig. 1).

Here we use a numerical model of crystal nucleation, growth, and dissolution to examine how crystal populations and zoning patterns record time-varying magmatic conditions in a water-saturated magma. The model results show that crystal resorption is common in magmas with fluctuations in temperature and, to a much lesser extent, pressure (pressure effects are primarily a reflection of dissolved water concentration in the melt). Moderate fluctuations in storage conditions can cause some crystal resorption, and larger excursions in temperature

* E-mail: andrewsb@si.edu. Orcid 0000-0001-9928-1225

0003-004X/21/0009–1438$05.00/DOI: https://doi.org/10.2138/am-2021-7491

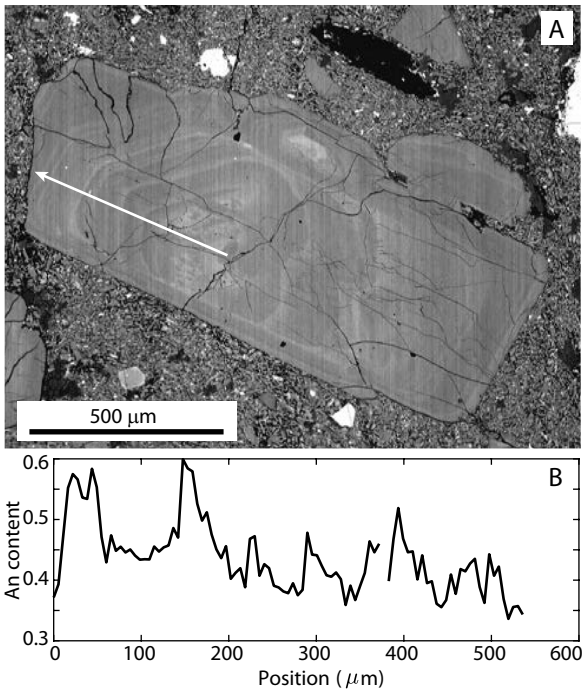

Figure 1. (**a**) BSE image of zoned plagioclase from sample El Chichón Unit E sample CHI9516 (1465–1520 yBP) with line indicating core-to-rim traverse. Age from Espindola et al. (2000). (**b**) Core-to-rim transect illustrating variation in anorthite content.

will likely resorb all small crystals. As a result, populations of smaller crystals most likely only record events subsequent to the most recent recharge event, and larger crystals generally preserve greater fractions of the total magmatic history. Importantly, resorption often removes substantial portions of the crystal record, such that much <50% of the total time interval may be preserved in crystals. Notably, the relationship between crystal thickness and time is not constant through the crystal record. Because most growth is accommodated during the relatively short intervals of cooling following a recharge or heating event, those intervals tend to be overrepresented in the crystals as compared to much longer periods spent at lower temperatures.

Background

Phenocrysts form (or dissolve) in response to thermodynamic disequilibrium, e.g., changes in pressure, temperature, oxygen fugacity, and/or composition. As a melt becomes supersaturated in a particular phase, that phase will nucleate and grow, whereas if a melt is undersaturated in a phase, that phase will dissolve (e.g., Ghiorso and Sack 1995; Gualda et al. 2012; Ghiorso and Gualda 2015). Nucleation, growth, and dissolution rates are controlled by the degree of disequilibrium, with high degrees of supersaturation or undersaturation resulting in faster rates (Donaldson 1985; Tsuchiyama 1985; Hammer and Rutherford 2002; Szramek et al. 2006; Andrews and Gardner 2010; Brugger and Hammer 2010; Mollard et al. 2012; Boehnke et al. 2013; Shea and Hammer 2013; Zhang and Xu 2016; Befus and Andrews 2018) with the caveat that very high melt viscosities, or other kinetic barriers, can effectively prevent crystallization or dissolution. Both growth and dissolution act to reduce disequilibrium such that crystallization or dissolution rate slows as the magma approaches equilibrium. Importantly, because the rates of growth and dissolution describe how fast a single-crystal face responds to disequilibrium, the evolution of those rates through time reflects the sum of growth or dissolution across the entire crystal population (Befus and Andrews 2018; Andrews and Befus 2020).

Plagioclase feldspar is often used to interpret magmatic histories because it is ubiquitous as a major mineral phase in arc magmas (e.g., Vance 1965; Nelson and Montana 1992; Singer et al. 1995; Davidson and Tepley 1997; Salisbury et al. 2008). The mineral is sensitive to changes in pressure, temperature, and melt composition, with more calcic (anorthitic) compositions occurring in higher temperature, higher pressure (particularly P_{H_2O}), and/or more mafic magmas. That compositional dependence has been exploited in numerous experimental studies to help determine pre-eruptive storage conditions (e.g., Rutherford et al. 1985; Gardner et al. 1995; Martel et al. 1999; Andrews and Gardner 2010; Sosa-Ceballos et al. 2014), and used to develop various geothermometers and plagioclase-melt hygrometers (e.g., Housh and Luhr 1991; Putirka 2005; Lange et al. 2009; Waters and Lange 2015). Importantly, the crystal structure of plagioclase, the coupled CaAl-NaSi substitution, and the slow intracrystalline diffusion of those species prevent homogenization of anorthite-albite zones, thus plagioclase compositional zoning can act as a proxy for the pressure-temperature-compositional history of a given crystal. This is in marked contrast to minerals with no major element sensitivity to those conditions, or those, like olivine, with comparatively fast internal diffusion that can remove most major element compositional zoning (Shea et al. 2019).

In general, concentrically zoned plagioclase crystals are interpreted to record episodes of increasing and decreasing temperature and/or pressure, as well as changes in magma composition (e.g., Singer et al. 1995; Davidson and Tepley 1997; Clynne 1999; Tepley et al. 1999, 2000; Wallace and Bergantz 2005; Andrews et al. 2008; Costa et al. 2008; Sosa-Ceballos et al. 2014). Crystal cores record older events than the subsequently formed rims, although sectioning effects can bias the sampled crystal population away from cores (Wallace and Bergantz 2005; Cheng et al. 2017).

Plagioclase zoning patterns are commonly interpreted as petrologic evidence for magma mixing or recharge (e.g., Eichelberger 1978; Tepley et al. 2000; Humphreys et al. 2006; Andrews et al. 2008; Sosa-Ceballos et al. 2014). Although recharge may act as an eruption trigger, many, perhaps even the majority of, recharge or mixing events do not result in eruption. El Chichón has erupted approximately the same composition of trachyandesite magma 7 times within the past ~3100 years, roughly equivalent to a ~500-year recurrence interval, but textural and compositional zoning patterns indicate that the magma reservoir is recharged much more frequently (Espindola et al. 2000; Tepley et al. 2000; Andrews et al. 2008). Those studies also indicate that many of the recharging magmas are compositionally very similar to the host trachyandesite. Sosa-Ceballos et al. (2014) suggest that Popocatépetl has intervals with more than 10 recharge events occurring within a decade and that most of those events are not accompanied by eruption.

Non-euhedral growth and crystal dissolution both act to complicate simple "tree-ring" interpretations of crystal zoning as described above. The dependence of growth texture on supersaturation (or undercooling) is explored in detail by Hammer and Rutherford (2002), who demonstrate that euhedral prismatic crystals only nucleate and grow under a limited set of conditions. Other workers have suggested that sieved plagioclase likely records growth during water-undersaturated decompression (Nelson and Montana 1992; Humphreys et al. 2006). Kawamoto (1992) shows that some patchy zoning in plagioclase may record initially skeletal habits, and Shea et al. (2019) have shown that some euhedral olivine crystals form through infilling of initially skeletal growth.

Partial or complete dissolution will occur when a mineral is introduced to a melt in which it is undersaturated (e.g., Donaldson. 1985; Tsuchiyama 1985; Ghiorso and Sack 1995; Boehnke et al. 2013; Zhang and Xu 2016). Dissolution can thus act to remove portions of the crystal record. Many workers have shown that dissolution surfaces are common in zoned crystals, with some crystals exhibiting repeated intervals of dissolution (e.g., Tepley et al. 1999; Salisbury et al. 2008; Streck et al. 2008). Unfortunately, although differential dissolution between different faces can provide estimates of the minimum amount of dissolution, the absolute amount of dissolution associated with each surface is usually unknown.

Because crystals are the result of time-integrated nucleation, growth, and dissolution processes, the compositional zoning profile of a given crystal can, in principle, be converted into a timeseries if growth and dissolution rates are known or assumed. Many previous experimental studies have described plagioclase nucleation and growth rates (e.g., Hammer and Rutherford 2002; Hammer 2004; Couch et al. 2003; Larsen 2005; Brugger and Hammer 2010; Shea and Hammer 2013; Befus and Andrews 2018), although most of those studies present time-averaged rates. Plagioclase dissolution rates, in contrast, are largely undescribed in the literature, with studies by Tsuchiyama (1985) showing that rates depend on crystal composition and Donaldson (1985) indicating that dissolution is approximately twice as fast as growth.

Various previous researchers have used numerical models to understand and interpret plagioclase zoning patterns, with many of these efforts focused on small amplitude and short length scale oscillatory zoning. Haase et al. (1980) use a compositionally dependent growth rate to show that oscillatory zoning can develop over a wide range of parameter space. L'Heureux and Fowler (1994) show that local disequilibrium at the interface between the crystal and melt drives crystallization, and oscillatory zoning can develop depending on the partition of material from the melt into the crystal and the relative growth and diffusion rates. Gorokhova et al. (2013) present a model of plagioclase rim growth during decompression that reproduces compositional zoning observed in samples erupted from Bezymianny. Notably none of those studies address crystal dissolution, the evolution of crystal populations through time, nor timescales substantially in excess of tens of days.

Numerical model of plagioclase nucleation, growth, and dissolution

We examine plagioclase crystallization and dissolution within an initially 1 m^3 model volume using a modified version of the numerical model SNGPlag (Andrews and Befus 2020); the model version presented in this study allows for much longer model runs, time-variant temperature and pressure, and crystal dissolution. Here, we briefly describe the original SNGPlag model before providing a detailed description of the new version. Following Befus and Andrews (2018) and Andrews and Befus (2020), we use the term "supersaturation" to describe the disequilibrium of the system, rather than "undercooling," as the former can be readily calculated or measured. Note that in this formulation, a negative supersaturation, or "undersaturation," refers to a system with an excess of crystals, e.g., a system in which crystals should dissolve.

SNGPlag Model

Supersaturation Nucleation and Growth of Plagioclase (SNGPlag) is an iterative numerical model that predicts plagioclase sizes and abundances as a function of magma composition, temperature, and decompression path; the model is fully discussed in Andrews and Befus (2020). At each time, t_i, SNGPlag evaluates the supersaturation, $\Delta\varphi$, as the difference between the plagioclase volume fraction, φ, at the previous time step and the equilibrium plagioclase volume fraction, φ_{eqb}, as predicted by MELTS at the specified time-dependent pressure and temperature, $P(t_i)$ and $T(t_i)$. Plagioclase volume fractions φ and φ_{eqb} are considered on a vesicle-free basis. Nucleation and growth rates, $I(t_i)$ and $J(t_i)$, are defined for the time step as functions of $\Delta\varphi$, as described by Befus and Andrews (2018). SNGPlag considers the plagioclase crystals to be rectangular prisms; at each time step, the axes grow by the amount $F\times J(t_i)\times\Delta t$, where F is a factor between 0 and 1 describing the ratio of the axis length to the c-axis length, and Δt is the time step. Growth is only applied to crystals or nuclei that exist in the previous step t_{i-1}. Nuclei are added to the model volume in the amount $I(t_i)\times\Delta t$. SNGPlag accounts for volumetric interferences between crystals through an analytical expression that does not allow two crystals to occupy the same volume (Andrews and Befus 2020); potential local variations in crystallization or dissolution rates arising from chemical gradients are not examined. Although the growth of real crystals in magmas does not usually result in perfect, rectangular prisms, particularly given the triclinic symmetry of plagioclase, analysis, and modeling of realistic textures (swallow tail, hopper, skeletal, etc.; Hammer and Rutherford 2002) for $>10^9$ crystals in the model volume is not feasible.

Modifications to SNGPlag

Whereas the previous version of SNGPlag examined isothermal decompression, we have changed the program to allow for more variable P-T conditions and longer model run times, permitting the study of magmatic processes in the reservoir prior to decompression and eruption. Specifically, the temperature can follow a prescribed path simulating isothermal (or near isothermal) conditions punctuated by a series of heating or recharge events. Similarly, the system can be isobaric or show fluctuations in pressure as might result from eruption of a portion of the reservoir (Segall 2016) or from circulation of a parcel of magma through higher and lower pressure regions (Anderson 1984); although we note that large variations in An content are unlikely to record repeated pressure cycling (Andrews et al. 2008; Sosa-Ceballos et al. 2014).

Crystals often reside within a magmatic system for durations of hundreds or thousands of years (e.g., Tepley et al. 1999, 2000; Cooper and Reid 2003; Andrews et al. 2008; Cooper and Kent 2014; Sosa-Ceballos et al. 2014; Budd et al. 2017), but nucleation and growth processes that affect those crystals can have timescales on the order of seconds to days (e.g., Gerlach and Grove 1982; Hammer and Rutherford 2002; Befus and Andrews 2018; Andrews and Befus 2020). That dynamic range, ~8 orders of magnitude, poses substantial challenges for a numerical model of crystallization; the previous version of SNGPlag is particularly hobbled, as a 1-year model run would require numerous 10- to 100-gigabyte matrices, and a 100-year run would generate files larger than 100 terabytes. To address this challenge, we calculate changes to the crystal population at fine temporal resolution (600 s), but only record those changes twice per day (Fig. 2). The addition of new crystals (through nucleation) and their subsequent growth is thus calculated every 600 s, producing a temporary population of 120 classes, each with its own a-, b-, and c-axis dimensions and N_v, every 12 h. That temporary population is then reduced to a single class through Equations 1–7.

$$V_i = \sum_{\tau=1}^{120} N_\tau L_{a\tau} L_{b\tau} L_{c\tau} \quad (1)$$

where the total volume V_i of crystals nucleated over the 120 time steps τ composing the 12 h time interval i–1 to i is the sum of the numbers N_τ and volumes (product of axis lengths $L_{x\tau}$) of crystals nucleated at each timestep τ.

$$N_i = \sum_{\tau=1}^{120} N_\tau \quad (2)$$

gives the total number of crystals N_i nucleated in the interval i–1 to i.

$$\nu_i = V_i/N_i \quad (3)$$

is the characteristic individual crystal volume.

$$V_\tau = \boldsymbol{N}_\tau L_{a\tau} L_{b\tau} L_{c\tau}/V_i \quad (4)$$

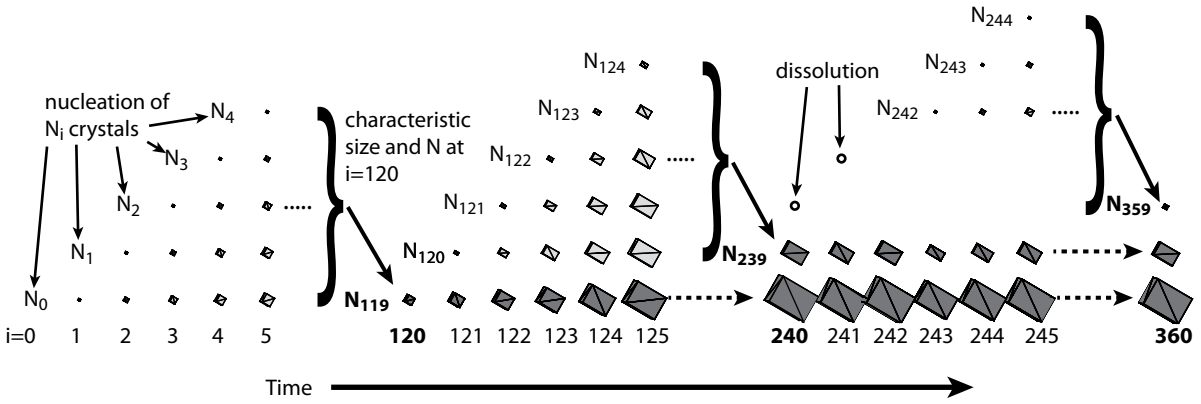

Figure 2. Schematic of SNGPlag crystal nucleation, growth, and dissolution. At each time t_i, N_i crystals can nucleate. Over the subsequent time step, those nuclei and all existing crystals grow (or dissolve) by growth rates dependent on supersaturation Δφ. To balance long model durations with computational limitations, temporary populations of newly nucleated crystals are tracked (light gray) at high temporal resolution, and then synthesized into a single-crystal class (dark gray) with characteristic size and number density N calculated every 120 time steps. Those "through-going" crystal classes continue to grow (or resorb) throughout the rest of the model run. Just as dissolution can eliminate crystals from the temporary populations, dissolution can also remove through-going crystals from the total population.

gives the fraction of new crystal volume (V_τ) that nucleated during each time step.

$$R_{\mathrm{aci}} = \sum_{\tau=1}^{120} V_\tau L_{a\tau} / L_{c\tau}$$
$$R_{\mathrm{bci}} = \sum_{\tau=1}^{120} V_\tau L_{b\tau} / L_{c\tau} \quad (5)$$

provides characteristic ratios of *a*- to *c*-axis and *b*- to *c*-axis lengths for crystals nucleated during the interval i–1 to i.

$$L_{\mathrm{ci}} = \left(\frac{v_{\mathrm{i}}}{R_{\mathrm{aci}} R_{\mathrm{bci}}} \right)^{1/3} \quad (6)$$

$$L_{\mathrm{ai}} = L_{\mathrm{ci}} R_{\mathrm{aci}}$$
$$L_{\mathrm{bi}} = L_{\mathrm{ci}} R_{\mathrm{bci}} \quad (7)$$

give the characteristic *c*-, *a*-, and *b*-axis lengths for all crystals nucleated during i–1 to i. The characteristic surface area of the crystals can be easily calculated as the product of the *a*-, *b*-, and *c*-axis lengths. Note that Equations 1–7 can be used to calculate characteristic crystal parameters of the total crystal population at any time by summing over the interval 1 to i for all crystals, rather than τ = 1 to 120 for only the temporary population.

The *c*-axis growth rates employed in the model are those described by Befus and Andrews (2018). The relative growth rates of the *a*- and *b*-axes are no longer constant fractions of the *c*-axis rate. Instead, relative crystal growth rates J_x vary linearly with Δφ, from equant or isotropic at Δφ = 0, to highly anisotropic at high supersaturations:

$$\mathrm{J_x} = (1 + \Delta\varphi m_{\mathrm{x}}) J_{\mathrm{c}} \quad (8)$$

where the subscript x denotes the *a*- or *b*-axis, and m_x describes deviation from equant growth; note that the *c*-axis growth rate does not vary linearly with Δφ. The parameter m_x is assumed to be –3 for *a* and –2 for *b*; although no systematic examination of m_x as a function of Δφ has been made, various experimental studies show that crystal morphologies are more elongate at high degrees of disequilibrium (e.g., Hammer and Rutherford 2002; Szramek et al. 2006) and the chosen values of m_x produce reasonable 3D crystal aspect ratios. This treatment of growth rate allows crystal morphology to vary with supersaturation, such that more equant crystals will grow at low Δφ and tabular or acicular crystals will form at high Δφ (the specific values of m_x are chosen to produce this result). We use the expression:

$$Sn_{\mathrm{i}} = \sum N_{\mathrm{i}} \left(L_{\mathrm{ai}}^{\,2} + L_{\mathrm{bi}}^{\,2} + L_{\mathrm{ci}}^{\,2} \right)^{1/3} \Big/ \sum N_{\mathrm{i}} \quad (9)$$

to obtain the characteristic crystal size at each time i. At each time i, the anorthite content (An) is determined using MELTS as a function of pressure and temperature, thus compositional information is associated with the *a*-, *b*-, and *c*-axis growth patterns within each crystal.

Numerous crystal textures indicate that crystal dissolution is an important and frequent process within many magmatic systems (Tepley et al. 1999, 2000; Andrews et al. 2008; Salisbury et al. 2008; Streck et al. 2008; Sosa-Ceballos et al. 2014). Importantly, the composition of plagioclase that is stable varies with pressure and temperature (e.g., Rutherford et al. 1985; Putirka 2005; Lange et al. 2009; Andrews and Gardner 2010; Sosa-Ceballos et al. 2014; Waters and Lange 2015; Waters et al. 2015), such that unless the system becomes superliquidus with respect to plagioclase, only certain compositions of plagioclase will dissolve (Tsuchiyama 1985). We assume that dissolution rate is a function of undersaturation (indicated by a negative Δφ), such that crystals will dissolve faster in highly undersaturated systems. More specifically, the dissolution rate follows the same functional form as the *c*-axis growth rate, but with a twofold increase in magnitude; for example, if Δφ = 0.1 results in a growth rate of ~0.2 μm/h, then Δφ = –0.1 results in a dissolution rate of ~0.4 μm/h. Experimental work by Tsuchiyama (1985) and Donaldson (1985) suggests that our simplifying assumption of

faster dissolution rates as compared to growth rates is reasonable. Recent papers combining experimental measurements of diffusion with measurements of zircon saturation (Boehnke et al. 2013; Zhang and Xu 2016) show that zircon dissolution rate rapidly increases as the zircon liquidus is exceeded; by applying their general findings to plagioclase, the dissolution rates of unstable plagioclase compositions should be expected to increase Δφ becomes increasingly negative. In addition, we assume dissolution rates are isotropic. Finally, to account for the potential stability of relatively higher An compositions of plagioclase (Tsuchiyama 1985), the model only permits dissolution of plagioclase with An less than the equilibrium value calculated by MELTS for the particular pressure and temperature at that time step.

Together, the Δφ-dependent anisotropic growth rates with Δφ- and An-dependent dissolution rates allows the model to grow complexly zoned crystals. A *P-T* trajectory resulting in increasing Δφ and decreasing An will produce a concentrically zoned crystal with a higher An core and lower An rim. If that crystal undergoes a dissolution event followed by renewed crystallization, the concentric zoning will be truncated with a greater fraction of the *a*- and *b*-axes dissolved compared to the *c*-axis (Fig. 3). Repeated episodes of dissolution and crystallization, such as might be expected to occur during and after recharge events, can produce crystals with oscillatory zoning in the *c*-axis and effectively monotonic zoning in the *a*- and/or *b*-axes (Fig. 3).

The new model allows a change in system volume during recharge events. As temperature increases, the system volume can increase by a specified fraction of crystal-free melt. This decreases the total crystallinity; for example, a volume increase of 0.1 decreases crystallinity by a factor of ~0.09 [= 1/(1 + 0.1)]. This volume addition is assumed to have an identical bulk composition as the original magma. Importantly, the fraction added does not imply that the volume of some magma reservoir increased by, for example, 10%, but that the volume in communication with the modeled crystals increased by that fraction. That is, a hypothetical 1 km^3 body of magma does not necessarily increase to 1.1 km^3, but some of the crystals experience a local increase in melt fraction and corresponding decrease in crystallinity.

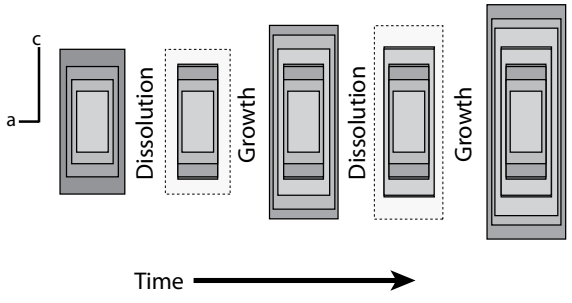

Figure 3. Schematic of crystal growth-resorption cycles, with higher An zones shown in lighter gray. Crystals grow at axis-specific rates proportional to supersaturation Δφ, with the effect of *c*-axis rates increasingly greater than *b*-axis rates that are in turn faster than *a*-axis rates. The net effect is to grow elongate or tabular crystals. Dissolution is assumed to occur at the same rates for all axes, but dissolution along a particular axis stops when a zone of stable An content is intersected. Repeated cycles of growth and dissolution result in zoned crystals. Not only are some portions of crystal history entirely removed from the record, the degree to which that erasure happens depends upon crystal axis.

As in the previously published version of SNGPlag, the new version of the model assumes that the other crystal phases are in instant equilibrium. In addition, the model does not account for changes in melt composition through time. Although tracking compositional changes during crystallization is trivial, calculating those changes during dissolution of compositionally zoned anisotropic crystals is beyond the scope of this project.

We use the nucleation and growth rates presented in Befus and Andrews (2018) as these are the only published instantaneous rates. All other published values are presented as time-averaged rates, generally as functions of the initial undercooling (Hammer and Rutherford 2002; Couch et al. 2003; Larsen 2005; Brugger and Hammer 2010; Shea and Hammer 2013). Use of time-averaged rates in an instantaneous model results in either impossibly large crystals and high crystallinities (applied to model durations of years or centuries such rates would produce meter-scale crystals in millimeter scale volumes of magma), or implausibly low crystallinities (when converted to time-variant rates). The "Timescales of equilibration and model sensitivity" section shows the effects of variation in nucleation, growth, and dissolution rates on model outputs.

For the purpose of this paper, we use the terms "antecryst," "phenocryst," and "microlite" following the definitions used in Andrews and Befus (2020). Antecrysts are crystals whose initial volumes do not affect the system equilibrium, although subsequent crystallization on antecrysts will affect equilibrium and thus Δφ. Phenocrysts are crystals present at the start of the run whose initial volume contributes toward equilibrium. A system can begin out of equilibrium but with a population of phenocrysts; for example, a system with $\varphi_{EQBplag} = 0.30$ could begin with $\varphi_{plag} = 0.15$, and would thus have 15 vol% phenocrysts but not yet be in equilibrium. A magma at superliquidus conditions can contain no phenocrysts, but could contain antecrysts. Microlites are defined as those crystals that nucleate and grow during the course of the simulation; although microlites are commonly associated with decompression, for the purpose of the model, they are any crystals that nucleate during initial equilibration or subsequent cooling and/or decompression. We note that with these definitions, there is little functional difference between phenocrysts and microlites in simulations with durations up to thousands of years, as the two groups of crystals can overlap in size and have similar zoning patterns.

Model results

We present the results of three suites of model runs using an El Chichón trachyandesite bulk composition with $\log(f_{O_2})$ = NNO+2.3 (Macias et al. 2003; Andrews et al. 2008; Table 1). First, we examine the response of the system to step-like changes in temperature to establish timescales over which a magma returns to equilibrium during 2-year model runs. These simula-

Table 1. Whole rock composition (in anhydrous wt%) of El Chichón trachyandesite used as input for MELTS and SNGPlag

SiO_2	TiO_2	Al_2O_3	FeO	MnO	MgO	CaO	Na_2O	K_2O	P_2O_5	Total	f_{O_2} ($\log_{10}$)
56.28	0.74	19.34	6.52	0.19	2.47	7.57	2.48	3.92	0.36	99.87	NNO+2.3

Note: Analysis from Macias et al. (2003) and Andrews et al. (2008).

tions act as simplified perturbation analyses of a more complex natural system. These results are further discussed in the context of model sensitivity to nucleation, growth, and dissolution rates. Second, we consider 2-year simulations with repeated cycles of heating-cooling or decompression-pressurization to better understand how populations of crystals survive intervals of crystallization and dissolution. Finally, we parameterize general model results and extend a simplified version of the model to a ~5300-year interval to study what fractions of magmatic history are preserved within a single crystal.

Timescales of equilibration and model sensitivity

Thermodynamic disequilibrium, quantified in SNGPlag as Δφ, drives crystallization or dissolution. We use model runs with step-like changes in temperature to rapidly increase the magnitude of Δφ and then examine how quickly the magma returns to or approaches equilibrium. After an initial dwell time of 182.5 days (0.5 year) at T_o, we change temperature to T_f over 1 day, and then hold at T_f for the remainder of the 2-year model run; runs with $T_f > T_o$ record negative values of Δφ, resulting in crystal dissolution, whereas runs with $T_f < T_o$ show positive excursions in Δφ, and thus crystal nucleation and growth. These runs have no volume addition during heating or cooling.

Figure 4a shows variation in Δφ with respect to time, and thus how quickly the modeled systems recover. The rate at which |Δφ| decreases is proportional to |Δφ|. Because the experimentally determined nucleation and growth rates are very low for Δφ < 0.04, reduction of the magnitude of Δφ to <<0.04 occurs slowly, with an asymptotic approach to Δφ = 0; this observation is further discussed in the "Application to natural systems" section. Not surprisingly, larger initial excursions in Δφ require longer times to recover. Although the instantaneous dissolution rate for any given crystal face is specified to be at least twice as fast as the growth rate for undersaturation and supersaturations with the same magnitude, the rates of system equilibration differ by less than a factor of 2, likely because dissolution acts on a decreasing number of crystals with decreasing size, whereas growth acts on an increasing number of ever larger crystals.

We examine the sensitivity of SNGPlag model results to nucleation, growth, and dissolution rates. For this sensitivity analysis, all rates follow the same functional form as those from Befus and Andrews (2018), but we vary the magnitudes from 25 times less (i.e., roughly comparable to rates reported by Hammer and Rutherford 2002) to 5 times greater. Figure 4b shows that slower nucleation and growth (or dissolution) rates, varied individually or jointly, result in slower return to equilibrium. Faster nucleation and growth (or dissolution) rates result in faster returns to equilibrium, with the decrease in response time approximately inversely proportional to the increase in rate. Changes in nucleation and growth rate both affect crystallization responses during intervals of supersaturation. Not surprisingly, the dissolution response during heating events is mostly sensitive to changes in dissolution rate (set by the growth rate), with minor sensitivity to nucleation rate, as that parameter affects the initial crystal population.

The time series for different magnitude heating or cooling events can be collapsed onto single trajectories for dissolution or crystallization. Specifically, time series with lower magnitude

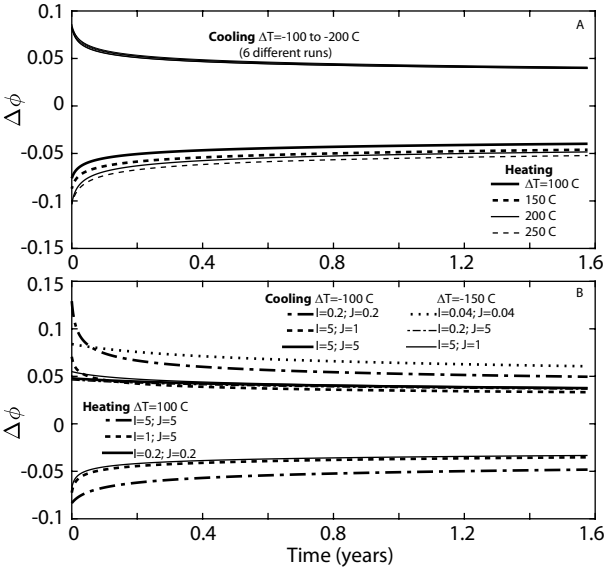

Figure 4. (**a**) Variation in supersaturation Δφ with time for step function changes in T with heating from T_o = 800 °C and cooling from T_o = 900 or 1000 °C. The cooling paths (with ΔT = 100, 150, and 200 °C) follow essentially identical decreases in Δφ. The heating paths show similar functional forms, but are offset by the differences between their initial Δφ. (**b**) Changes in the magnitudes of nucleation (I) and growth or dissolution rates (J) strongly affect how quickly a magma returns to equilibrium. The rate at which a system returns to equilibrium is proportional to both I and J during crystallization, but mostly dependent upon J during dissolution.

Δφ can be overlain onto the highest magnitude Δφ series by introducing a lag in the time indices of the lower Δφ series. The magnitude of supersaturation (or undersaturation) decreases approximately linearly as a function of supersaturation (or undersaturation) in log-log space. Crystallinity (expressed as supersaturation or undersaturation) does not vary exponentially with time; that is, there is not a simple "half-life" expression to describe how quickly the magma returns to equilibrium. These patterns indicate that the times over which magmatic systems return to a near-equilibrium state are a function of the maximum disequilibrium experienced by the system and that Δφ can be used to predict the instantaneous rate of system crystallization or dissolution when the nucleation, growth, and dissolution rates are known. Although this predicted response is not quite as precise as the full model, it can be used to inform longer-duration models of crystallization ("Modeling longer run durations" section).

Not surprisingly, nucleation, growth, and dissolution rates strongly affect the fidelity with which individual crystals record the magma history. Online Material[1] OM1 shows the sensitivity of crystal zoning patterns to variation in nucleation, growth, and dissolution rates from 25 times less to 10 times greater than those reported by Befus and Andrews (2018). Those tests show that elevated growth rates produce large crystals that record large time fractions (>70% in the test scenario) when nucleation rate is low, with changes in dissolution rate only causing minor differences in the crystal record. High nucleation rates result in low fractions of recorded time (~10%) even at high growth rates. The fraction

of recorded time varies inversely with covariation in nucleation, growth, and dissolution rates such that for elevated or nominal values, the crystals record ~10% of the scenario, but preserved time fraction increases to ~18 and ~37% as the rates increase to 0.1 and 0.04 times the nominal values, respectively. Low growth rates result in small crystals; complete dissolution of such crystals is common during the modeled heating or recharge events except when nucleation and dissolution rates were both reduced.

Repeated oscillations in temperature and/or pressure

Thermal cycling. We examine cycles of magma heating and cooling, analogous to a conceptual model of the thermal effects of recharge on a host magma, by introducing repeated heating-cooling cycles. We begin with a host magma at an initial temperature T_o that is then heated to a higher temperature T_f, before returning to F_t. The temperature-time series follows a Gaussian trajectory described by the error function; heating of the magma in this scenario occurs ~3 times more rapidly than cooling such that, for example, a heating event with total duration above T_o equal to 60 days achieves a maximum temperature after 15 days. For brevity, here we discuss four time series, each with three heating events. The initial equilibrium crystal fraction plagioclase for all of these runs is 0.413, and the runs begin with φ_{plag} = 0.265 (or 50% of $\varphi_{EQBplag}$) comprising equal fractions of cubic crystals of sizes 200, 150, 100, and 75 μm. Presentation of 3D crystal shape is discussed in Online Material[1] OM2.

Figure 5 shows results from a 2-year model run at T_o = 800 °C with 100 °C heating events, each lasting for 60 days, with no volume addition, occurring at 6, 12, and 18 months; such events can be thought of as resulting from underplating by hotter magma. During each event, crystallinity decreases during heating and increases as the system cools. The population of crystals changes markedly over the course of the model run, such that a maximum number of crystals is present immediately before the initiation of each recharge event (and at the end of the model run), and minimum numbers are present during intervals with the highest temperatures. Most of the crystals that form do not survive subsequent recharge events. The crystal population always comprises a small number of phenocrysts and a small subset of early nucleated crystals, with a subordinate number of crystals that nucleate and resorb until the final thermal maximum is achieved (Figs. 5c and 5d). As a consequence, the characteristic crystal dimensions (Fig. 5e) are dominated by the early formed crystals with only minor excursions from stable values reflecting the nucleation and resorption of new crystals; the crystal size Sn, however, shows step changes as those crystals come and go. The characteristic shape for all crystals (Fig. 5f) shows a gradual elongation through time, reflecting effectively isotropic resorption followed by non-isotropic (e.g., c>b>a axis) growth; note that the shape for newly grown crystals is more elongate and oscillates over the same range through each cycle.

Figure 6 shows a run with identical conditions as presented in Figure 5, but with a volume addition of 0.25 during each heating event. The additional system volume decreases the plagioclase volume fraction during heating, leading to a reduced magnitude of undersaturation. The slower dissolution rates and the reduced total amount of dissolution allow survival of more crystals from preceding recharge episodes, with nearly all crystals nucleated

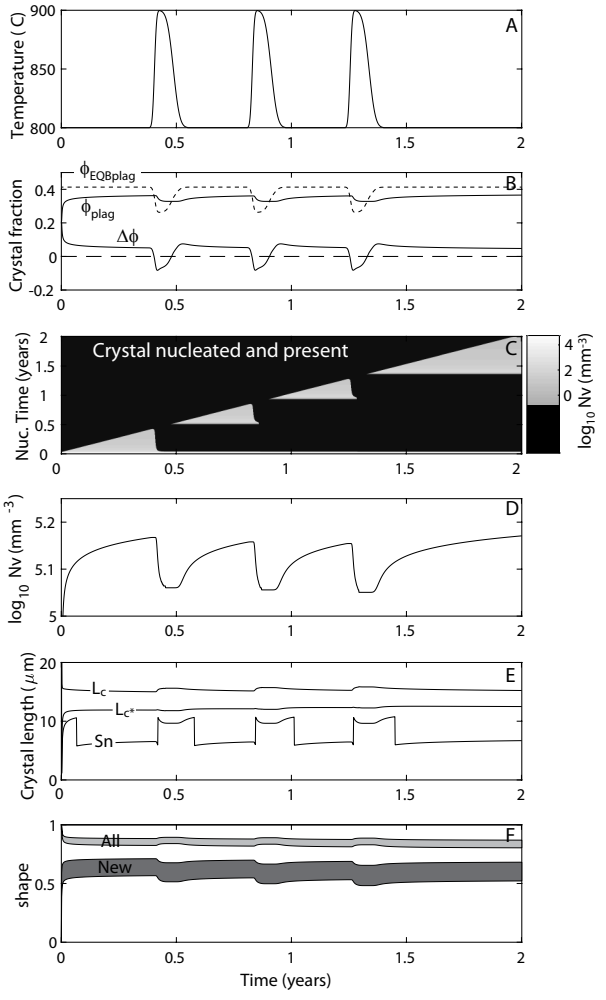

Figure 5. Two-year SNGPlag run with no volume addition at P = 100 MPa. (**a**) Temperature-time series. (**b**) Equilibrium ($\varphi_{EQBplag}$) and calculated (φ_{plag}) plagioclase crystal fractions and supersaturation ($\Delta\varphi$). (**c**) Survival diagram showing when crystals nucleate and their residence time in the magma. (**d**) Plagioclase number density N_v. (**e**) Characteristic crystal size Sn and lengths L_a, L_b, L_c. (**f**) Characteristic crystal shape for all crystals ("All") at each time and only those nucleated during the model run ("New"). The upper line indicates the ratio of *b*- to *c*-axis length, and the lower line *a*- to *c*-axis length; the two lines together thus describe how equant, tabular, or elongate the crystals are. This method of plotting shape is explained in detail in Online Material[1] OM2.

prior to the first heating event, and a portion of those nucleated after the first thermal maximum, surviving to the end of the model run (Fig. 6c). The preservation of a more diverse crystal population also damps the step-like variations in the Sn time series (Fig. 6e). Characteristic crystal shape shows similar evolution through time, with crystals becoming more elongate (Fig. 6f).

Crystal growth following heating events is proportional to volume fraction input, and the amount of dissolution during those events scales inversely with the added volume fraction (Fig. 7). Volume addition thus makes zones larger and reduces their subsequent dissolution. The effects of increased system volume during heating events also appear in the compositional

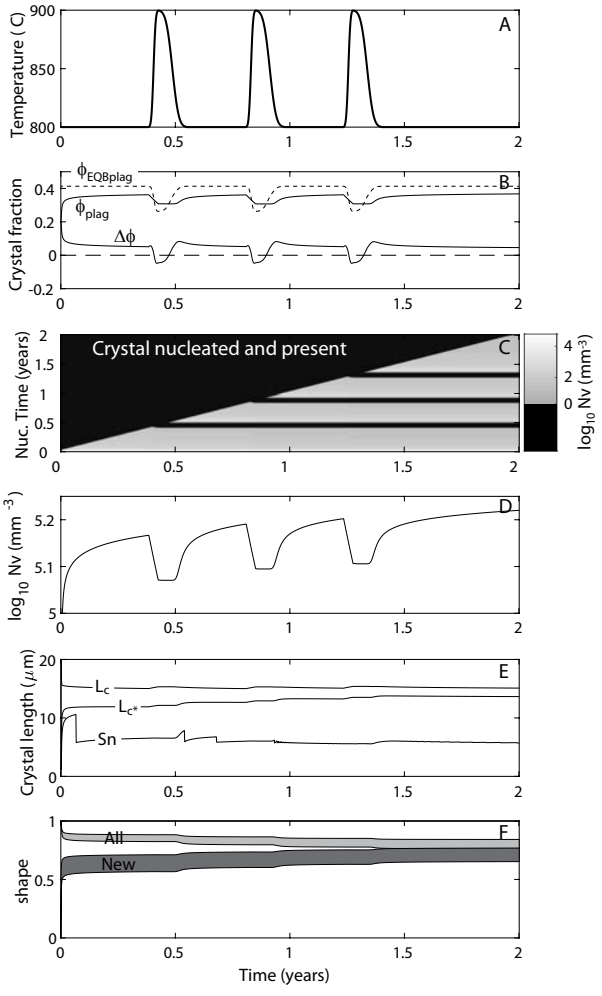

Figure 6. Two-year SNGPlag run with 0.25 volume fraction addition during each heating event. (**a**) Temperature-time series. (**b**) Equilibrium ($\varphi_{EQBplag}$) and calculated (φ_{plag}) plagioclase crystal fractions and supersaturation ($\Delta\varphi$). (**c**) Survival diagram showing when crystals nucleate and their residence time in the magma. (**d**) Plagioclase number density N_v. (**e**) Characteristic crystal size Sn and lengths L_a, L_b, L_c. (**f**) Characteristic crystal shape for all crystals at each time ("All") and only those nucleated during the model run ("New").

zoning of crystals. Figure 8 shows *a*-, *b*-, and *c*-axis transects of An content and the times that are recorded in a crystal nucleated at day 1 for the scenarios shown in Figures 5 and 6. Although the *c*-axis profiles for both crystals show 3 peaks in An content, the scenario with volume addition preserves 2 peaks in the *a*- and *b*-axes. Evaluated in the context of the intervals preserved by each axis, it becomes apparent that the specified volume addition enabled preservation of the *a*- and *b*-axis zones grown following the first heating event—a fraction of crystal that was completely dissolved during the scenario with no volume addition.

Given that not all recharge events should be the same temperature or affect all regions of the host magma with the same magnitude and duration of temperature excursion, we examine 2-year model runs with 120 d recharge events of increasing and decreasing thermal magnitudes (Fig. 9). For these simulations, volume addition during each recharge event is 0.1. In systems with increasing temperatures, no crystals nucleated following one recharge event survive the next recharge event; in other words, the 200 °C event dissolves all post 150 °C crystals, and the 250 °C event dissolves all crystals formed after the 200 °C thermal maximum. In contrast, the model run with decreasing magnitudes of recharge events preserves a large number of crystals; specifically, all crystals formed above 200 °C during cooling following the first thermal maximum survive until the end of the run, as do all formed above 150 °C during cooling following the second thermal maximum. The characteristic plagioclase sizes and shapes evolve differently for the increasing and decreasing series. In the increasing series, Sn evolves strong peaks during the heating events, reflecting dissolution of all but the largest crystals, whereas in the decreasing series Sn remains low after the first event because some small crystals survive each heating event. Similarly, characteristic shape shows more variation through time in the increasing series and finishes with slightly more elongate morphology than the decreasing series; again, this is the result of more crystals surviving through the decreasing series.

Pressure cycling. Pressure within a magma reservoir may drop during eruption (e.g., Anderson 1984; DeGruyter and Huber 2014; Segall 2016; Townsend et al. 2019). With the magnitude of decrease, and the timescale over which pressure returns to its initial value, being functions of numerous factors including magma and host rock compressibility, and the ratio of erupted volume to reservoir volume (Huppert and Woods 2002; DeGruyter and Huber 2014; Segall 2016; Townsend et al. 2019). In addition, if a magma convects, then crystals within the magma may record changes in pressure (Anderson 1984). Here we consider comparatively rapid decompression events as generated by eruptions that are then followed by more gradual increases in pressure that

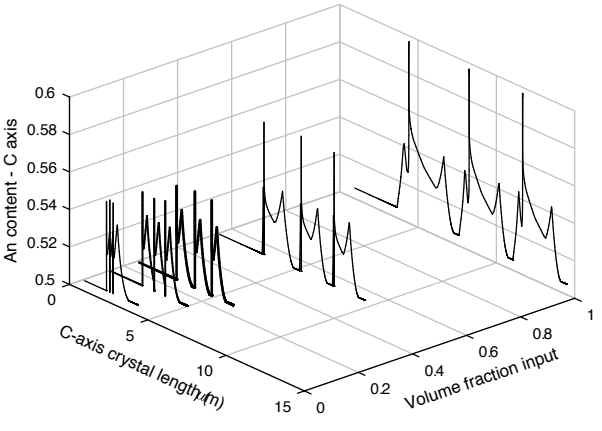

Figure 7. Effects of different volume additions V_{input} during otherwise identical SNGPlag runs with three 60 day duration 150 °C heating events from T_o = 750 °C. With V_{input} = 0, only the peak An values from the first two events survive. As V_{input} increases, the three recharge events become more distinct in the crystal record. At V_{input} > 0.25, some crystallization from between the recharge events is preserved. The double-peaked structure in the zoning patterns results from MELTS calculating non-monotonic variation in An content between 750 and 800 °C at 100 MPa.

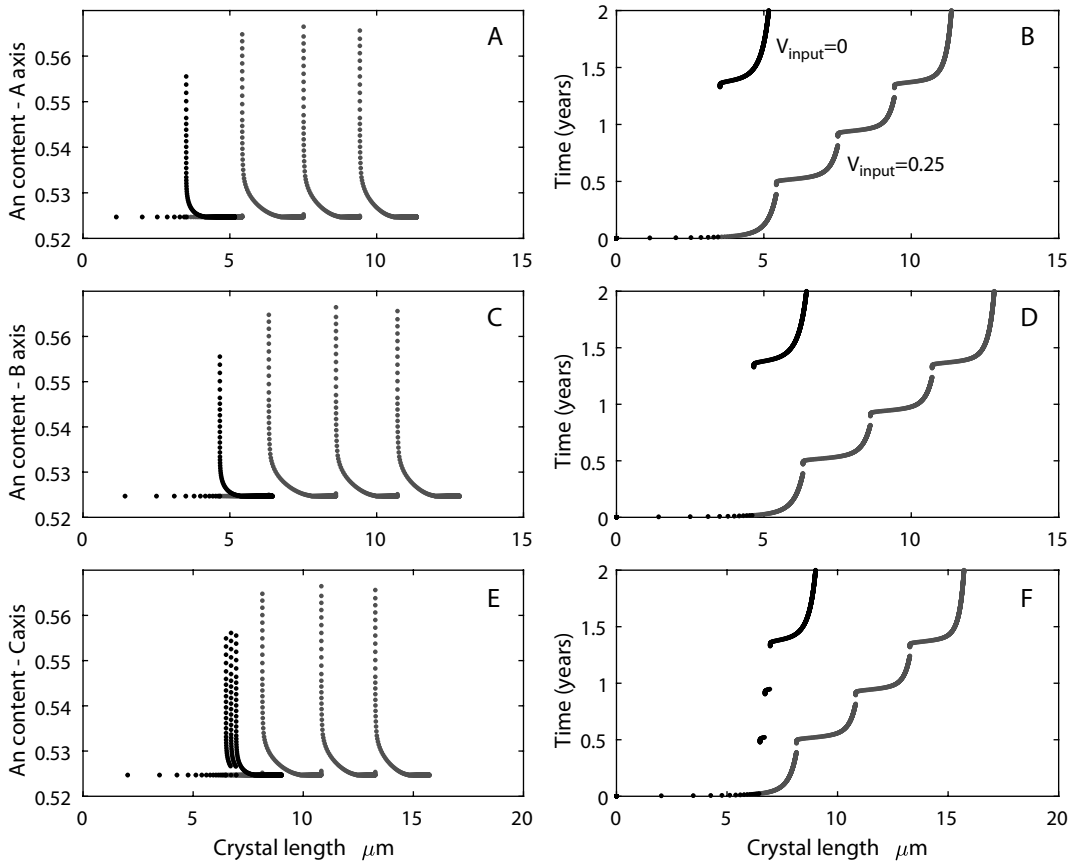

Figure 8. Modeled compositional zoning patterns and time intervals recorded by crystals nucleated at t = 1 day for the scenarios shown in Figures 6 and 7. Model runs with V_{input} = 0 record very little zoning in the *a*- and *b*-axes (panels **a**–**d**), whereas those with V_{input} = 0.25 show well-developed zones and virtually no missing time intervals. The *c*-axis shows zoning in both scenarios, although the zones are highly compressed (**e**) and have substantial time missing for the V_{input} = 0 condition (**f**).

return the system to its initial pressure. We assume a *P-t* path that follows the same functional form as the recharge events, with the minimum pressure being achieved at 25% of the total cycle duration. During each decompression-pressurization cycle, no magma volume is added to the system. We note here that as Δφ is the driving parameter for the SNGPlag model, a decompression event could be recast as a cooling event, that is, both result in an initial increase in Δφ (resulting in crystallization) followed by a decrease in Δφ (potentially resulting in dissolution).

Figure 10 shows the *P-t* path for a sequence of three decompressions from 100 to 50 MPa at 800 °C with event durations of 120 days. We note that these drops are of larger magnitude than should be expected during most eruptive cycles, but are roughly comparable in the magnitude of induced Δφ as cooling from 800 to ~750 °C; smaller amplitude, more geologically plausible decompressions, manifest virtually no crystallization record in the model. In contrast to the heating events, pressure cycling begins with a positive change in Δφ, resulting in crystal nucleation and growth. The system remains plagioclase supersaturated during repressurization (Δφ remains positive), thus although nucleation and growth rates decrease, the system never resorbs crystals. This lack of resorption is the combined result of pressure cycles with durations comparable to or less than the timescales required for achieving equilibrium, and decompression inducing relatively small amplitude changes in Δφ (each decompression cycle only increases Δφ by ~0.03 or less). Were the pressure cycles larger in magnitude and longer in duration, then some crystal dissolution would be expected during the later stages of repressurization.

Modeling longer run durations

The previously discussed runs have had 2-year durations, with one 10-year simulation used to examine how the systems approach equilibrium over a longer duration. Magmatic processes, however, often occur over much longer intervals, and individual crystals can record processes with durations that exceed thousands or tens of thousands of years (Cooper and Reid 2003; Andrews et al. 2008; Cooper and Kent 2014; Sosa-Ceballos et al. 2014; Budd et al. 2017). We use the timescales of equilibration determined in the "Timescales of equilibration and model sensitivity" section to develop a simplified model of plagioclase disequilibrium Δφ as a function of pressure-temperature-time path. That time series of Δφ allows us to calculate the growth, dissolution, and compositional history of a single crystal over a geologically interesting interval. Here

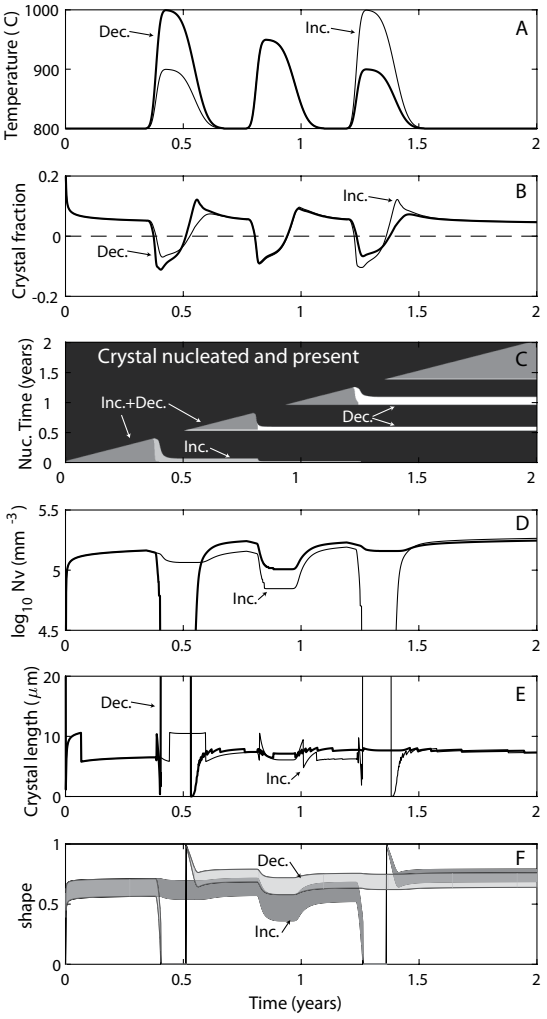

Figure 9. SNGPlag results for sequences of heating events with increasing ("Inc.") or decreasing ("Dec.") magnitude. (**a**) Temperature time series. (**b**) Supersaturation Δφ. (**c**) Survival diagram. (**d**) Crystal number density N_v. (**e**) Characteristic crystal size (Sn) and *c*-axis length (L_c). (**f**) Characteristic crystal shape for crystals nucleated during the two runs. In all panels, the heavy line represents the increasing series and the thin line the decreasing series.

we describe that simplified model, validate it against a 5-year run of SNGPlag to ensure that it can recover results of the full model run, and then use it to examine a hypothetical ~5300-year pressure-temperature-time series.

Supersaturation Δφ is the difference between the equilibrium volume fraction plagioclase, as determined by MELTS, and the modeled plagioclase fraction. Consequently, at a constant equilibrium crystallinity φ_{EQB}, the rate at which Δφ changes (Δφ/dt) describes the crystallization rate of that system. The equilibration times series discussed in the "Timescales of equilibration and model sensitivity" section and displayed in Figure 4 show $\Delta\varphi/dt$ is proportional to Δφ. If plagioclase crystallinity, φ, is assumed, then Δφ at that time can be calculated as $\Delta\varphi = \varphi_{EQB} - \varphi$, which can be used to determine $\Delta\varphi/dt$ at that time. That rate then determines the amount of crystallization (or dissolution) that occurs during the next time step. At that new time t_i, the difference between φ and φ_{EQB} determines Δφ, and the model thus proceeds iteratively, as shown in the expression:

$$\varphi_i = \varphi_{i-1} + (\Delta\varphi/dt)_{i-1}\Delta t \quad (10)$$

Although this iterative approach may accumulate uncertainty, the timescales required for equilibration are on the order of hundreds of days, thus intervals spent at constant temperature for more than a few hundred days (e.g., on the order of 1 year or less) should prevent forward propagation of those errors.

We validate this approximation of the full model by comparing it to a 5-year run of SNGPlag. The runs have a series of convolved excursions in temperature and pressure (Fig. 11), allowing us to examine plagioclase population dynamics over a range of temperature, pressure, and time scales. Comparison of

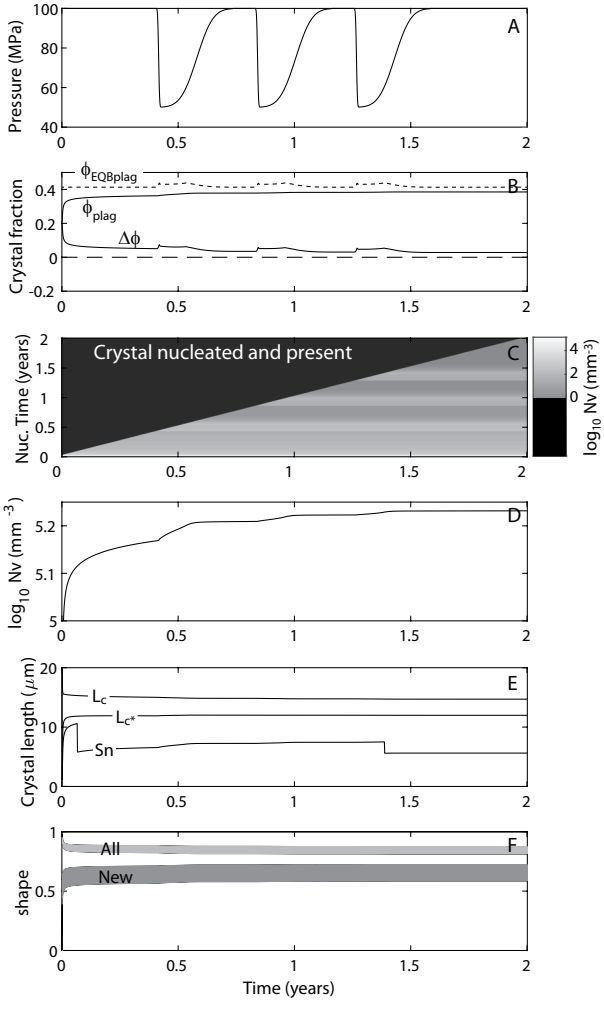

Figure 10. A 2-year SNGPlag run at 800 °C. (**a**) Pressure time series. (**b**) Equilibrium ($\varphi_{EQBplag}$) and calculated (φ_{plag}) plagioclase crystal fractions and supersaturation (Δφ). (**c**) Survival diagram showing when crystals nucleate and their residence time in the magma. (**d**) Plagioclase number density N_v.

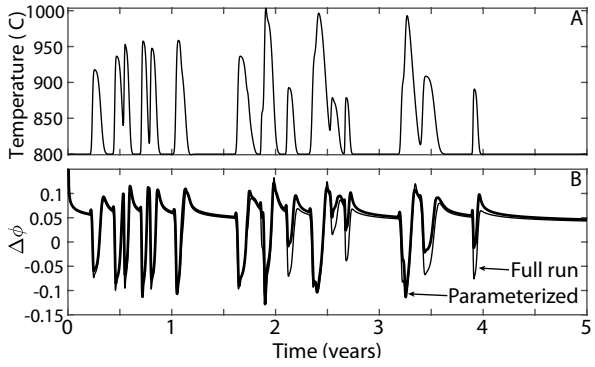

Figure 11. (**a**) A 5-year temperature-time series used in full and parameterized SNGPlag run. (**b**) Comparison of supersaturation, Δφ, values for parameterized and full SNGPlag runs conducted with same parameters. Because Δφ controls crystallization and dissolution rates, good agreement between Δφ for the two model runs indicates that the parameterized run accurately reproduces the crystallization record for a single crystal as calculated by the full run.

Δφ between the full and simplified runs shows good agreement (Fig. 11). Because the parameter Δφ controls crystallization and dissolution, that agreement indicates that the parameterized version of the model accurately captures the processes as calculated by the full model.

We now consider a hypothetical magma body over ~5300 year with a randomly generated magma recharge and eruption history. Series of recharge events occur every 200 years (Fig. 12). Each series can last from 10–100 years, with up to 5 events per decade. Those events have 50–150 °C magnitudes, durations of 0.25–10 years, volume fraction additions of 0–0.5, and can be superimposed upon one another. Each series of recharge events can also have an eruption, that is, an interval of 10–25 MPa decompression over up to 7 days, with the system returning to its initial pressure (100 MPa) over 0.25–10 years. The initial pressure is at the lower bound of likely storage pressures for the Chichón trachyandesite (Macias et al. 2003) or other intermediate arc magmas but is chosen as it allows for a larger thermal range of plagioclase stability and An contents than higher pressures. The modeled interval contains a total of 454 recharge events and 12 decompressions or eruptions occurring in 26 groups. These values are not chosen to mimic any specific volcano or series of eruptions but rather to examine a geologically reasonable family of recharge and eruption scenarios (Andrews and Manga 2014; Cooper and Kent 2014; Sosa-Ceballos et al. 2014; Segall 2016). Runs at higher pressures show a systematic decrease in the fraction of time preserved in crystals as the same temperature excursions induce greater magnitude |Δφ| and potentially more time spent at or above the plagioclase liquidus.

Figure 13 shows the final compositional zoning profile predicted from the modeled *P-T-t* series. Online Material[1] OM3 shows an animation of the compositionally zoned crystal, illustrating growth, dissolution, and compositional profiles through time. In model runs with zero or low volume additions during heating events, the system repeatedly crystallizes and dissolves variations of the same zone, thus no net growth occurs (Online Material[1] OM4). Each heating-cooling episode results in possible dissolution followed by crystallization of initially higher An plagioclase followed by decreasing An plagioclase, thus we should expect each episode to be recorded by a rapid or step-like increase in An content, followed by a more gradual decrease. Moving outward from the core, ~20 distinct An peaks can be recognized with step-like increases of >10 mol% preserved in the record. This number is markedly lower than the >400 total recharge events in the temperature time series (Fig. 12). The lower number of recorded events is not surprising as some of the modeled recharge events are superimposed on one another, resulting in effectively singular events, and because dissolution during some episodes removes preceding portions of the crystal record. In addition, the crystal is completely resorbed twice during the first 2000 years, as can be seen in the obliteration of

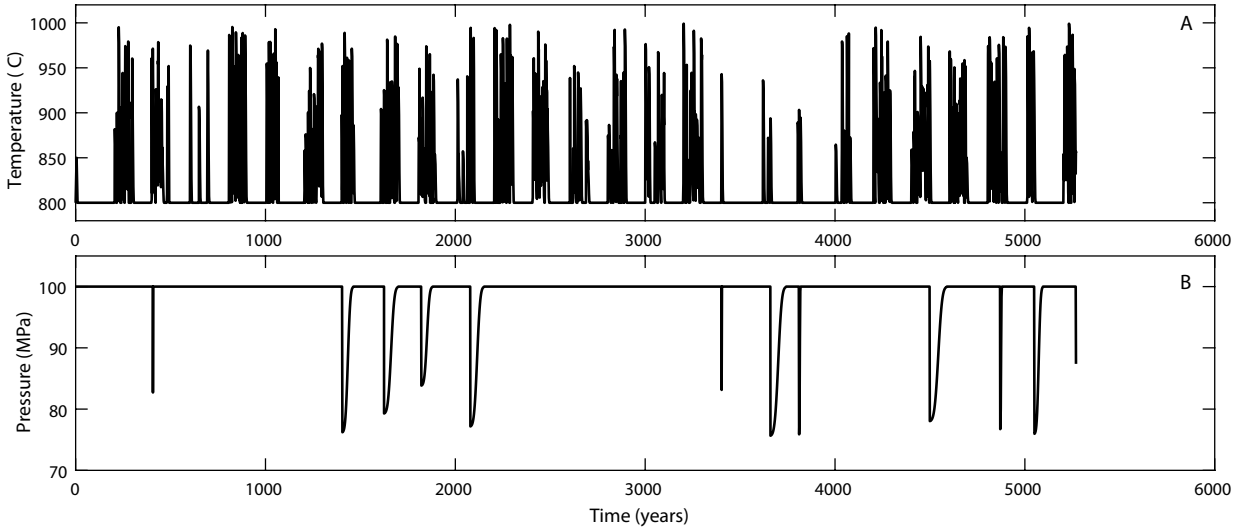

Figure 12. (**a**) Temperature and (**b**) pressure series for the 5269-year run. The run comprises 454 heating events and 12 decompressions or eruptions in 26 groups.

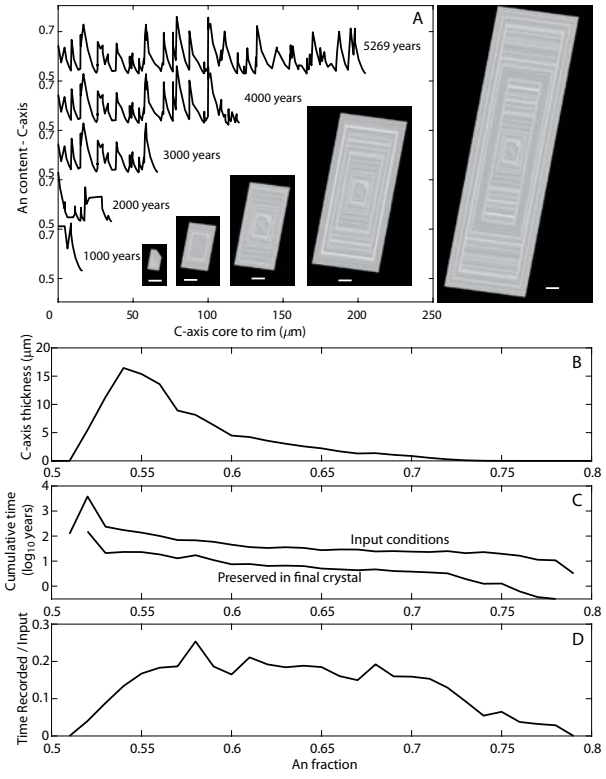

Figure 13. (**a**) *C*-axis core-to-rim transects during 5269-year time series, and pseudo-backscattered electron sections through the growing crystal. (**b**) Histogram showing cumulative thickness as a function of composition for the final (5269 year) crystal with bin size of 0.01 An fraction. (**c**) Input and recorded (crystallized) conditions shown as histogram of time with bin sizes of 0.01 An fraction. (**d**) The ratio of time recorded to time spent as a function of pressure-temperature conditions (and thus An content).

crystal zones grown during that period (Fig. 13).

The numerical results show that the ~5300-year magmatic history is not uniformly sampled by the crystal (Fig. 13). Qualitatively, the more complete zoning patterns preserved in the *c*- vs. *a*- and *b*-axes show that possibly large fractions of the crystal record are missing. Not only are intervals of dissolution missing from the crystal record, but that record is dominated by intervals of high supersaturation during which faster growth occurs; such intervals occur as the parcel of magma cools following each recharge event. This has the effect of undersampling higher temperature and lower temperature intervals (that is, intervals crystallizing the highest and lowest An compositions). A histogram of An composition indicates that the range of *P-T* conditions recorded by the crystal approximates the range of equilibrium conditions experienced by the magma, but its distribution is not proportional to the time spent at those conditions (Fig. 13).

Discussion

SNGPlag predicts how a population of plagioclase crystals will evolve in response to changes in pressure and temperature. In general, heating or pressurization results in dissolution, whereas cooling or decompression result in crystal nucleation and growth. More anorthitic plagioclase forms at elevated pressures and temperatures. Thus an individual recharge event is likely recorded as a step-like increase in An content, followed by a more gradual decline. Because the model conditions dissolution on An content, a high-An zone can shield more inboard regions of a crystal from dissolution. The net results of these nucleation, growth, and dissolution processes are that smaller, more albitic plagioclase more easily dissolves than larger plagioclase with more anorthitic zones and that high-temperature excursions will often dissolve crystals (or zones) formed during preceding lower temperature intervals, including recharge events of smaller thermal magnitude.

The model shows that, in general, large crystals survive for longer intervals than, and effectively grow at the expense of, smaller crystals. This process is not Ostwald ripening, but rather the interplay of outward growth and inward dissolution rates of crystal faces. We note here that growth and dissolution have units of distance per time, as these processes occur through the incremental addition or removal of atoms from faces of individual crystals; defining these rates with units of volume (or volume fraction) per time presupposes a crystal number density and size distribution. The same growth rate applied to large and small crystals crystallizes much more material onto the former, more rapidly reducing supersaturation and retarding additional nucleation and growth. Larger crystals are more likely to contain high-An zones that can shield more albitic interiors. Consequently, smaller crystals completely dissolve more readily than large crystals, such that repeated cycles of dissolution and crystallization can have the effect of "ratcheting up" the size of crystals that survive dissolution.

Net growth requires mass addition

If the modeled system has no additions of crystal mass (or volume), then those crystals (or zones) formed during the initial crystallization event and/or those formed during some final temperature decrease are most likely to be preserved; crystals formed during earlier, lower temperature intervals will be dissolved. This means that oscillatory zoning with compositional ranges >10 mol% An (and perhaps less) is unlikely to form only through the cycling of temperature and/or pressure but also requires the addition of mass to the system.

The addition of mass to the modeled system during recharge events has the effect of reducing the total crystallinity, thereby reducing the magnitude of plagioclase undersaturation (i.e., reducing the magnitude of $\Delta\varphi$). Although dissolution can still occur during an episode of heating, this "dilution" of the system crystallinity effectively allows the magma to crystallize a larger final fraction than initially dissolved (i.e., 9 vol% dissolves during heating, but 10 vol% crystallizes during the subsequent cooling). Without mass addition, the same zones grow and resorb over and over again during temperature or pressure cycling, thus oscillatory or complex zoning cannot develop.

This required mass addition does not mean that the total magma reservoir increases in volume by, for example, a factor of 0.1, only that the volume interacting with the crystal(s) of interest increases. In addition, the new mass need not be directly from the recharging magma but could be remobilized host magma. This further highlights how two crystals might record the same

event very differently (Andrews et al. 2008; Sosa-Ceballos et al. 2014): a crystal near enough to the recharging magma to see the addition of new mass would initially experience dissolution before the growth of a new zone for a net increase in crystal size, whereas a more distal crystal might only experience dissolution followed by a roughly equivalent amount of growth resulting in effectively no net change in crystal size. Analysis of trace element zoning, in tandem with An zoning, could provide a means of identifying whether the mass added to the local system is remobilized from the host or is new magma entering the system; the former would likely show little or no change in trace element concentrations, whereas the latter should show variability in trace elements correlated with the An zoning.

Application to natural systems

The model results discussed in this paper are not intended to precisely mimic a specific natural system. Although the simulations presented here were all performed using El Chichón trachyandesite composition, the actual Chichón magma system has processes and characteristics beyond consideration of this model, including mixing of different composition magmas, assimilation of host rock, and multiple crystal populations. Further, this model assumes dissolution rates and depends on growth rates that are reasonable but not experimentally verified for Chichón. Despite those simplifications, the model offers insights into the dynamics of natural magma processes. In addition, the parameterized model ("Modeling longer run durations" section) can be applied to an arbitrary magma composition by, for example, using MELTS to determine the plagioclase volume fraction and composition as functions of pressure and temperature.

First, because crystal growth and dissolution rates are very low at small degrees of disequilibrium, plagioclase crystallization and dissolution are not particularly sensitive to small changes in pressure, temperature, or composition. This does not mean that, for example, no nucleation or growth will occur when a magma cools by 5 °C (equivalent to increasing $\Delta\varphi$ by ~0.01 or less), but that crystallization will proceed exceptionally slowly. Indeed, whereas large excursions in disequilibrium will return to $|\Delta\varphi| < 0.05$ in hundreds of days, reduction in the magnitude of $\Delta\varphi$ to <0.02 (i.e., further approaching thermodynamic equilibrium) requires times in excess of 150 years; even if that second timescale is too long, the general pattern of asymptotic approach to equilibrium holds, and magmas should show limited response to small changes in $\Delta\varphi$. This is not to suggest that magma bodies do not cool (or heat) over much longer timescales, but that crystallization (or dissolution) will keep pace and maintain equilibrium, or a state near equilibrium, with any changes in intensive parameters occurring over timescales greater than hundreds of days.

Second, substantial amounts of time are likely missing from the record of any given crystal. That missing time is the result of both changing rates of crystallization, including protracted periods with very slow growth rates, as well as dissolution. Indeed, it is not unreasonable for 50% of a total crystal thickness to have formed during 10% of its history and 75% of its total history to be missing through the result of dissolution. This observation is similar to the "cold storage" hypothesis of Cooper and Kent (2014), where magmas may spend substantial fractions of time in a cool, rheologically locked, uneruptible state, but with the important extension that some intervals are entirely removed from individual crystals. Our results show that the plagioclase crystallization record is biased against high-temperature intervals, although more limited information describing high-temperature thermal state may be preserved by diffusion profiles within crystals, such as duration and magnitude of heating. Future work, involving a large number of model runs with *P-T-t* paths informed by other petrologic observations and numerical models (e.g., Andrews et al. 2008; DeGruyter and Huber 2014; Sosa-Ceballos et al. 2014; Townsend et al. 2019) could serve to quantify the bias in the crystallization record as a function of recharge volumes, and recharge and eruption frequencies.

Third, the *c*-axis preserves a more complete record than other crystallographic axes. This is true not only because the faster-growing axis will stretch zoning patterns compared to the *a*- and *b*-axes, but also because dissolution may completely remove zones from faces normal to the *a*- and *b*-axes. Previous workers have noted that the *c*-axis provides the best opportunity to correlate crystals (e.g., Wallace and Bergantz 2002, 2004, 2005). Such correlations are very complicated as sectioning artifacts can remove crystal cores from the observed section (Wallace and Bergantz 2005; Cheng et al. 2017), and different crystals may record the same event differently based upon, for example, their proximity to the recharging magma (Andrews et al. 2008). Moreover, relative motions between crystals will change their crystallization/dissolution responses to subsequent events. As with previous workers (Wallace and Bergantz 2002, 2005; Cheng et al. 2017), we suggest that correlation is most likely to succeed by working from the outside in and that large numbers of crystals must be examined. Further, we suggest that robust correlations require matching both the shape and magnitude because they record separate, albeit related, aspects of magma history: the change in An content (i.e., "magnitude") provides an indication of the absolute change in temperature (or composition of the melt), whereas the shape of a zone records system disequilibrium ($\Delta\varphi$) through time.

Implications

Our model suggests that the crystal record is biased against higher and lower An compositions and toward more recent time intervals. That is, although the range in plagioclase composition may reflect the range in pressure-temperature-composition experienced by the magma, the fraction of high- to low-An zones does not record the relative time spent at those conditions. In addition, the smallest crystals likely only record time since the most recent dissolution event.

Substantial intervals of time are not recorded by phenocrysts. Depending upon the amount of mass addition that occurs in close proximity to a crystal during recharge or heating events, dissolution can erase and slow growth rates can compress large fractions of a crystal's history. Together those processes can effectively remove more than 50% of time from a crystal record.

Complex compositional zoning in plagioclase requires mass addition as well as heating. Significant heating with little or no mass addition will likely result in substantial dissolution and obliteration of the crystal record. The common occurrence of complex compositional zoning indicates that most heating events experi-

enced by individual crystals, or at least most that are preserved in the crystal record, are accompanied by the addition of new melt.

Mixed crystal populations are ubiquitous in arc andesites and dacites. The compositional range in any given crystal records the pressure-temperature-composition-time (*P-T-X-t*) conditions that the crystal experienced, but that history may not be representative of the magma in general. Obtaining a unified *P-T-X-t* history of a magma requires reconciling the disparate records of many different crystals. Different crystals will likely record different magmatic histories, even if they are only mm apart at the time of eruption. The complexity in resolving the disparate histories recorded by separate crystals should indicate the timescales and length scales of processes within the magma body: large and prolonged events affecting the entire magma body should be recorded more uniformly than small scale events that are, perhaps, only recorded by those crystals in close physical proximity to the disturbance.

Finally, crystal populations approach equilibrium with magma intensive parameters over timescales of hundreds of days. This indicates that the crystal populations effectively maintain textural (and compositional) equilibrium during processes operating over timescales greater than approximately 1 year (e.g., gradual heating or cooling of a magma body). This also suggests that the lag between the onset of some rapid or dynamic process and the crystallization response of the magma(s) occurs over timescales shorter than hundreds of days. For example, the interval during which neither an initially hotter intruding magma and cooler host magma are sufficiently crystallized to be rheologically locked must be substantially less than 100 days; thus fluid mixing (or mingling) of compositionally and/or thermally distinct magmas must occur relatively quickly during recharge events.

Acknowledgments

The SNGPlag model benefited from helpful discussions with K.S. Befus, M.S. Ghiorso, and G. Sosa-Ceballos. C. Huber and A. Kent provided thoughtful reviews that improved this manuscript.

References cited

Anderson, A.T. (1984) Probable relations between plagioclase zoning and magma dynamics, Fuego Volcano, Guatemala. American Mineralogist, 69, 660–676.

Andrews, B.J., and Befus, K.S. (2020) Supersaturation nucleation and growth of plagioclase: A numerical model of decompression induced crystallization. Contributions to Mineralogy and Petrology, 175, 23. https://doi.org/10.1007/s00410-020-1660–9.

Andrews, B.J., and Gardner, J.E. (2010) Effects of caldera collapse on conduit dimensions and magma decompression rate: An example from the 1800 ^{14}C yr BP eruption of Ksudach Volcano, Kamchatka, Russia. Journal of Volcanology and Geothermal Research, 198, 205–216.

Andrews, B.J., and Manga, M. (2014) Thermal and rheological controls on the formation of mafic enclaves or banded pumice. Contributions to Mineralogy and Petrology, 167, 961.

Andrews, B.J., Gardner, J.E., and Housh, T.B. (2008) Repeated recharge, assimilation, and hybridization in magmas erupted from El Chichón as recorded by plagioclase and amphibole phenocrysts. Journal of Volcanology and Geothermal Research, 175, 415–426.

Befus, K.S., and Andrews, B.J. (2018) Crystal nucleation and growth produced by continuous decompression of Pinatubo magma. Contributions to Mineralogy and Petrology, 173, 92. doi.org/10.1007/s00410-018-1519–5.

Boehnke, P., Watson, E.B., Trail, D., Harrison, T.M., and Schmitt, A.K. (2013) Zircon saturation revisited. Chemical Geology, 351, 324–334.

Browne, B.L., Eichelberger, J.C., Patino, L.C., Vogel, T.A., Uto, K., and Hoshizumi, H. (2006) Magma mingling as indicated by texture and Sr/Ba ratios of plagioclase phenocrysts from Unzen volcano, SW Japan. Journal of Volcanology and Geothermal Research, 154, 103–116.

Brugger, C.R., and Hammer, J.E. (2010) Crystal size distribution analysis of plagioclase in experimentally decompressed hydrous rhyodacite magma. Earth and Planetary Science Letters, 300, 246–254.

Budd, D.A., Troll, V.R., Deegan, F.M., Jolis, E.M., Smith, V.C., Whitehouse, M.J., Harris, C., Freda, C., Hilton, D.R., Halldórsson, S.A., and Bindeman, I.N. (2017) Magma reservoir dynamics at Toba caldera, Indonesia, recorded by oxygen isotope zoning in quartz. Scientific Reports, 7, 40624.

Cheng, L., Costa, F., and Carniel, R. (2017) Unraveling the presence of multiple plagioclase populations and identification of representative two-dimensional sections using a statistical and numerical approach. American Mineralogist, 102, 1894–1905.

Clynne, M.A. (1999) A complex magma mixing origin for multiple volcanic lithologies erupted in 1915 from Lassen Peak, California. Journal of Petrology, 40, 105–132.

Cooper, K.M., and Kent, A.J.R. (2014) Rapid remobilization of magmatic crystals kept in cold storage. Nature, 506, 480–483.

Cooper, K.M., and Reid, M.R. (2003) Re-examination of crystal ages in recent Mount St. Helens lavas: Implications for magma reservoir processes. Earth and Planetary Science Letters, 213, 149–167.

Costa, F., Chakraborty, S., and Dohmen, R. (2003) Diffusion coupling between trace and major elements and a model for calculation of magma residence times using plagioclase. Geochimica et Cosmochimica, 67, 2189–2200.

Costa, F., Dohmen, R., and Chakraborty, S. (2008) Time scales of magmatic processes from modeling the zoning patterns of crystals. Reviews in Mineralogy and Geochemistry, 69, 545–594.

Couch, S., Sparks, R., and Carroll, M. (2003) The kinetics of degassing-induced crystallization at Soufriere Hills Volcano, Montserrat. Journal of Petrology, 44, 1477–1502.

Davidson, J.P., and Tepley, F.J. III (1997) Recharge in volcanic systems: Evidence from isotope profiles of phenocrysts. Science, 275, 826–829.

Davidson, J., Tepley, F. III, Palacz, Z., and Meffan-Main, S. (2001) Magma recharge, contamination and residence times revealed by in situ laser ablation isotopic analysis of feldspar in volcanic rocks. Earth and Planetary Science Letters, 184, 427–442.

DeGruyter, W., and Huber, C. (2014) A model for eruption frequency of upper crustal silicic magma chambers. Earth and Planetary Science Letters, 403, 117–130.

Donaldson, C.H. (1985) The rates of dissolution of olivine, plagioclase, and quartz in a basalt melt. Mineralogical Magazine, 49, 683–693.

Eichelberger, J.C. (1978) Andesitic volcanism and crustal evolution. Nature, 275, 21–27.

Espindola, J.M., Macias, J.L., Tilling, R.I., and Sheridan, M.F. (2000) Volcanic history of El Chichón Volcano (Chiapas, Mexico) during the Holocene, and its impact on human activity. Bulletin of Volcanology, 62, 90–104.

Gardner, J.E., Rutherford, M.J., Carey, S., and Sigurdsson, H. (1995) Experimental constraints on pre-eruptive water contents and changing magmatic storage conditions prior to explosive eruptions of Mount St. Helens volcano. Bulletin of Volcanology, 57, 1–17.

Gerlach, D.C., and Grove, T.L. (1982) Petrology of Medicine Lake Highland Volcanics: Characterization of endmembers of magma mixing. Contributions to Mineralogy and Petrology, 80, 147–159.

Ghiorso, M.S., and Gualda, G.A.R. (2015) An H_2O-CO_2 mixed fluid saturation model compatible with rhyolite-MELTS. Contributions to Mineralogy and Petrology, 169, 53.

Ghiorso, M.S., and Sack, R.O. (1995) Chemical mass transfer in magmatic processes. IV. A revised and internally consistent thermodynamic model for the interpolation and extrapolation of liquid-solid equilibria in magmatic systems at elevated temperatures and pressures. Contributions to Mineralogy and Petrology, 119, 197–212.

Gorokhova, N.V., Melnik, O.E., Plechov, P.Yu., and Shcherbakov, V.D. (2013) Numerical simulation of plagioclase rim growth during magma ascent at Bezimianny Volcano, Kamchatka. Journal of Volcanology and Geothermal Research, 263, 172–181.

Gualda, G.A.R., Ghiorso, M.S., Lemons, R.V., and Carley, T.L. (2012) Rhyolite-MELTS: A modified calibration of MELTS optimized for silica-rich, fluid-bearing magmatic systems. Journal of Petrology, 53, 875–890.

Haase, C.S., Chadam, J., Feinn, D., and Ortoleva, P. (1980) Oscillatory zoning in plagioclase feldspar. Science, 209, 272–274.

Hammer, J.E. (2004) Crystal nucleation in hydrous rhyolite: Experimental data applied to classical theory. American Mineralogist, 89(11-12), 1673–1679.

Hammer J.E., and Rutherford M.J. (2002) An experimental study of the kinetics of decompression-induced crystallization in silicic melt. Journal of Geophysical Research, 107(B1), ECV 8-1–ECV 8-24. doi:10.1029/2001JB000281.

Housh, T.B., and Luhr, J.F. (1991) Plagioclase-melt equilibria in hydrous systems. American Mineralogist, 76, 477–492.

Humphreys, M., Blundy, J.D., and Sparks, R.S.J. (2006) Magma evolution and open-system processes at Shiveluch Volcano: Insights from phenocryst zoning. Journal of Petrology, 47, 2303–2334.

Huppert, H., and Woods, A. (2002) The role of volatiles in magma chamber dynamics. Nature, 420, 493–495.

Kawamoto, T. (1992) Dusty and honeycomb plagioclase: indicators of processes in the Uchino stratified magma chamber, Izu Peninsula, Japan. Journal of Volcanology and Geothermal Research, 49, 191–208.

L'Heureux, I., and Fowler, A.D. (1994) A nonlinear dynamical model of oscillatory zoning in plagioclase. American Mineralogist, 79, 885–891.
Lange, R.A., Frey, H.M., and Hector, J. (2009) A thermodynamic model for the plagioclase-liquid hygrometer/thermometer. American Mineralogist, 94, 494–506.
Larsen, J.F. (2005) Experimental study of plagioclase rim growth around anorthite seed crystals in rhyodacite melt. American Mineralogist, 90, 417–427.
Macias, J.L., Arce, J.L., Mora, J.C., Espindola, J.M., Saucedo, R., and Manetti, P. (2003) A 550-year-old Plinian eruption at El Chichón Volcano, Chiapas, Mexico: Explosive volcanism linked to reheating of the magma reservoir. Journal of Geophysical Research, 108(B12), 2569. doi:10.1029/2003JB002551.
Martel, C., Pichavant, M., Holtz, F., Scaillet, B., Bourdier, J.-L., Traineau, H. (1999) Effects of f_{O2} and H_2O on andesite phase relations between 2 and 4 kbar. Journal of Geophysical Research, 104, 29453–29470.
Mollard, E., Martel, C., and Bourdier, J.-L. (2012) Decompression-induced crystallization in hydrated silica-rich melts: Empirical models of experimental plagioclase nucleation and growth kinetics. Journal of Petrology, 53(8), 1743–1766.
Nelson, S.T., and Montana, A. (1992) Sieve-textured plagioclase in volcanic rocks produced by rapid decompression. American Mineralogist, 77, 1242–1249.
Putirka, K. (2005) Igneous thermometers and barometers based on plagioclase+ liquid equilibria: Tests of some existing models and new calibrations. American Mineralogist, 90, 336–346.
Rutherford, M.J., Sigurdsson, H., Carey, S., and Davis, A. (1985) The May 18, 1980, eruption of Mount St. Helens 1. Melt composition and experimental phase equilibria. Journal of Geophysical Research, 90, 2929–2947.
Salisbury, M.J., Bohrson, W.A., Clynne, M.A., Ramos, F.C., and Hoskin, P. (2008) Multiple plagioclase crystal populations identified by crystal size distributions and in situ chemical data: Implications for timescales of magma chamber processes associated with the 1915 eruption of Lassen Peak, CA. Journal of Petrology, 49, 1755–1780.
Segall, P. (2016) Repressurization following eruption from a magma chamber with a viscoelastic aureole. Journal of Geophysical Research, 121, 8501–8522.
Shea, T., and Hammer, J.E. (2013) Kinetics of cooling-and decompression-induced crystallization in hydrous mafic-intermediate magmas. Journal of Volcanology and Geothermal Research, 260, 127–145.
Shea, T., Hammer, J.E., Hellebrand, E., Mourey, A.J., Costa, F., First, E.C., Lynn, K.J., and Melnik, O. (2019) Phosphorous and aluminum zoning in olivine: contrasting behavior of two nominally incompatible elements. Contributions to Mineralogy and Petrology, 174, 85.
Singer, B.S., Dungan, M.A., and Layne, G.D. (1995) Textures and Sr, Ba, Mg, Fe, K and Ti compositional profiles in volcanic plagioclase: Clues to the dynamics of calc-alkaline magma chambers. American Mineralogist, 80, 776–798.
Sosa-Ceballos, G., Gardner, J.E., and Lassiter, J.C. (2014) Intermittent mixing processes occurring before Plinian eruptions of Popocateptl volcano, Mexico: Insights from textural-compositional variations in plagioclase and Sr-Nd-Pb isotopes. Contributions to Mineralogy and Petrology, 167, 966.
Streck, M.J., Broderick, C.A., Thornber, C.R., Clynne, M.A., and Pallister, J.S. (2008) Plagioclase populations and zoning in dacite of the 2004–2005 Mount St. Helens eruption: Constraints form magma origin and dynamics. U.S. Geological Survey Professional Paper, 1750, 791–808.
Szramek, L., Gardner, J.E., and Larsen, J. (2006) Degassing and microlite crystallization of basaltic andesite magma erupting at Arenal Volcano, Costa Rica. Journal of Volcanology and Geothermal Research, 157, 182–201.
Tepley, F.J. III, Davidson, J.P., and Clynne, M.A. (1999) Magmatic interactions as recorded in plagioclase phenocrysts of Chaos Crags, Lassen volcanic center, California. Journal of Petrology, 40, 787–806.
Tepley, F.J. III, Davidson, J.P., Tilling, R.I., and Arth, J.G. (2000) Magma mixing, recharge and eruption histories recorded in plagioclase phenocrysts from El Chichón Volcano, Mexico. Journal of Petrology, 41, 1397–1411.
Townsend, M., Huber, C., Degruyter, W., and Bachmann, O. (2019) Magma chamber growth during inter-caldera periods; insights from thermo-mechanical modeling with applications to Laguna del Maule, Campi Flegrei, Santorini, and Aso. Geochemistry, Geophysics, and Geosystems, 20, 1574–1591.
Tsuchiyama, A. (1985) Dissolution kinetics of plagioclase in the melt of the system diopside-albite-anorthite, and the origin of dusty plagioclase in andesites. Contributions to Mineralogy and Petrology, 43, 243–270.
Vance, J.A. (1965) Zoning in igneous plagioclase: Patchy zoning. Journal of Geology, 73, 636–651.
Wallace, G.S., and Bergantz, G.W. (2002) Wavelet-based correlation (WBC) of crystal populations and magma mixing. Earth and Planetary Science Letters, 202, 133–145.
——— (2004) Constraints on mingling crystal populations from off-center zoning profiles: A statistical approach. American Mineralogist, 89, 64–73.
——— (2005) Reconciling heterogeneity in crystal zoning data: An application of shared characteristic diagrams at Chaos Crags, Lassen Volcanic Center, California. Contributions to Mineralogy and Petrology, 149, 98–112.
Waters, L.E., and Lange, R.A. (2015) An updated calibration of the plagioclase-liquid hygrometer-thermometer applicable to basalts through rhyolites. American Mineralogist, 100, 2172–2184.
Waters, L.E., Andrews, B.J., and Lange, R.A. (2015) Rapid crystallization of plagioclase phenocrysts in silicic melts during fluid-saturated ascent: Phase equilibrium and decompression experiments. Journal of Petrology, 56, 981–1006. doi:10.1093/petrology/egv025.
Zhang, Y., and Xu, Z. (2016) Zircon saturation and Zr diffusion in rhyolitic melts, and zircon growth speedometer. American Mineralogist, 101, 1252–1267.

Manuscript received February 24, 2020
Manuscript accepted October 17, 2020
Manuscript handled by Julie Roberge

Endnote:

[1]Deposit item AM-21-97491, Online Material. Deposit items are free to all readers and found on the MSA website, via the specific issue's Table of Contents (go to http://www.minsocam.org/MSA/AmMin/TOC/2021/Sep2021_data/Sep2021_data.html).